Hindawi
Shock and Vibration
Volume 2022, Article ID 4330043, 8 pages
https://doi.org/10.1155/2022/4330043

Research Article

Numerical Study on the Water Entry Impact Forces of an Air-Launched Underwater Glider under Wave Conditions

Xiangcheng Wu,[1] Xin Chang,[1] Shewen Liu,[1] Pengyao Yu,[1] Lilei Zhou,[2] and Wei Tian[3]

[1]*Naval Architecture and Ocean Engineering College, Dalian Maritime University, Dalian, China*
[2]*Dalian Shipbuilding Industry Offshore Co., LTD, Dalian, China*
[3]*No. 719 Research Institute of China State Shipbuilding Company Limiteo, Wuhan, China*

Correspondence should be addressed to Xin Chang; changxin_heu@outlook.com

Received 30 December 2021; Revised 10 March 2022; Accepted 24 March 2022; Published 12 April 2022

Academic Editor: Desmond Adair

In this study, the water entry of an air-launched underwater glider under wave conditions is numerically simulated by the computational fluid dynamics method. The numerical model is validated by the comparison of nondimensional water entry impact force with published experimental and numerical results. And the influence of water entry points, water entry angles, and water entry attack angles on impact force is studied, which provides guidance for the design of air-launched underwater gliders. The results show that the water entry point has a great influence on the peak value of vertical impact force. In the present study, the peak value of the maximum vertical impact force at different water entry points is almost twice the minimum peak value with the same water entry velocity. The water entry angle at the same water entry point has great influence on the peak value of horizontal impact force, which is mainly related to the horizontal component of the impact velocity. The greater the horizontal component of impact velocity, the greater the peak value of impact force. In addition, the attack angle hardly affects the water entry impact force of the glider with hemispherical head.

1. Introduction

The underwater glider is a kind of autonomous underwater vehicle which has been broadly applied in physical and biological oceanography [1]. At present, underwater gliders are mainly deployed by ships. Limited by the navigation capacity of the mother ship, long-distance deployment takes a long time. In contrast, air launched from the aircraft can greatly shorten the time required for long-distance deployment [2]. However, the water entry of the air-launched underwater glider is a complex process. During water entry, the air-launched underwater glider will suffer a huge impact force that can damage the structure and inner components [3]. Therefore, it is necessary to study the water entry impact force of the air-launched underwater glider.

The theoretical research on water entry can be traced back to Karman [4]. Based on the theory of potential flow, von Karman calculated the impact loads of a structure into water. Wagner [5] refined the theory of von Karman by taking the piled-up water surface and spray thickness into consideration. Miloh [6] used the semi-Wagner approach to compute the wetting factor and slamming coefficient of a rigid sphere in vertical water entry. Korobkin [7] constructed an exact solution for the problem of an elliptical paraboloid entering an ideal, incompressible liquid at variable velocity within framework of the Wagner approximation and examined the effect of the shape on peak impact accelerations. Tassin et al. [8] analyzed the accuracy of several models for prediction of the hydrodynamic loads by comparing with the experimental observation data.

With the development of computer simulation technology, many computational fluid dynamics (CFD) techniques have been used to study the impact problems of water entry. Aquelet et al. [9] presented the prediction of the local high-pressure load on a rigid wedge impacting a free surface, where the fluid was represented by solving the Navier–

Stokes equations with an arbitrary Lagrange Euler (ALE) formulation. Panciroli et al. [10] studied the hydroelastic phenomena during the water entry of elastic wedges by the numerical model which is based on the coupled finite element method (FEM) and smoothed particle hydrodynamics (SPH) formulation. The results show that the numerical solutions agree reasonably well with the experimental data. Facci et al. [11] used the finite volume method (FVM) to discretize incompressible Navier–Stokes equations in both air and water and describe the free-surface multiphase flow by the method of volume of fluid (VOF). This method is proved to be reasonable and feasible in simulating the three-dimensional water entry of a solid body. Large eddy simulation (LES) can well calculate the problem of multiphase flow [12–14]. Li et al. used LES to study the problem of a stone impacting on the water. And the numerical model is verified to be reasonable by comparing the numerical results with experimental results [15].

Subsequently, scholars applied CFD techniques to the water entry study of air-launched autonomous underwater vehicles (AUVs). Shi et al. [16] and Chaudhry et al. [17] investigated the water entry process of air-launched AUV by the software LS-DYNA based on the ALE method. The simulation results such as cavity shape and impact loads show good agreement with experimental data. Yan et al. [18] studied the small-angle water entry problem of the AUV numerically by the FEM-SPH coupling algorithm. This method absorbs the advantages of SPH algorithm in dealing with large deformation and meshes distortion. CFD technology can also accurately simulate the problem of AUV entering water. Qi et al. [19] simulated the water entry process of air-launched AUVs. A series of accurate load data were obtained and the accompanied phenomena such as cavitation were observed. Wang et al. [20] simulated the high-speed water entry of AUVs with asymmetric nose shapes. The trajectory and cavity development were accurately simulated.

As reviewed above, the CFD technology has been proved to be a reasonable and feasible method to study the water entry problem. To our knowledge, previous studies mainly focused on the impact forces of AUV onto the static water and the effect of waves on the water entry impact forces of AUV has not been fully investigated. In this study, the water entry impact forces of an air-launched underwater glider under wave conditions are studied by the CFD method. The water entry impact forces at different water entry points and different water entry angles are studied. The results can provide a reference for the design of air-launched underwater gliders.

The study is organised as follows. Section 2 introduces the numerical model. Section 3 verifies the accuracy of the present numerical model. Section 4 analyses the water entry impact forces of an air-launched underwater glider in different water entry points, water entry angles, and attack angles. Section 5 summarises the main conclusions.

2. Numerical Model

2.1. Governing Equations. The commercial CFD software STAR-CCM+ is employed to solve the water entry impact forces in this paper. The unsteady Reynolds Averaged Navier–Stokes (RANS) equations are discretized by using FVM. It is assumed that the fluid is incompressible and the temperature is constant. Then, the continuity equation and the NS equations can be written as

$$\nabla \cdot \mathbf{u} = 0,$$
$$\frac{\partial \mathbf{u}}{\partial t} + (\mathbf{u} \cdot \nabla)\mathbf{u} = -\frac{1}{\rho}\nabla p + \nu \nabla^2 \mathbf{u} + \mathbf{F}, \tag{1}$$

where $\mathbf{u}$ is the velocity vector, ρ is the fluid density, p is the fluid pressure, ν is the fluid kinematic viscosity, and $\mathbf{F}$ is the volume force.

The method of VOF is used to capture the free-surface multiphase flow. In each grid, the sum of the volume fraction of air phase and water phase is 1.0. Suppose the volume fraction of air is γ and the volume fraction of water is $1 - \gamma$. Then, the free surface can be tracked by solving the volume fraction of air phase, and the governing equation can be expressed as [21]

$$\frac{\partial \gamma}{\partial t} + \nabla \cdot \left(\gamma \mathbf{v_r}\right) = 0, \tag{2}$$

where $\mathbf{v_r}$ is the transfer velocity.

There are three possible conditions in every grid as follows:

$$\gamma = \begin{cases} 0, & \text{if grid is full of water,} \\ 1, & \text{if grid is full of air,} \\ 0 < \gamma < 1, & \text{if grid contains both water and air.} \end{cases} \tag{3}$$

Then, the air and water in every grid can be regarded as an equivalent fluid with the density ρ_e and the viscosity ν_e calculated by

$$\rho_e = \gamma \rho_a + (1 - \gamma)\rho_w,$$
$$\nu_e = \gamma \nu_a + (1 - \gamma)\nu_w, \tag{4}$$

where ρ_a and ρ_w are the density of air and water, respectively, and ν_a and ν_w are the dynamic viscosity of air and water, respectively.

In addition, the motion of the structure is computed by Newton's second law. The motion of the grid around the structure is realized by overset mesh method. The transfer of physical quantities between the overset zone and the background zone is employed by the linear interpolation method.

2.2. Air-Launched Underwater Glider Model. In this study, an air-launched underwater glider model is proposed to study the water entry problem, which is shown in Figure 1. The traditional underwater glider has a large wingspan to improve the lift force during gliding. And the wing bears a large impact force in the process of water entry. So, a new design scheme, equipping a foldable wing module on the top of the underwater glider, is proposed to reduce the water entry impact force in this paper. During the impact into water, the wing is folded, as shown in Figure 1(a). After entering the water, the velocity of the glider decreases and

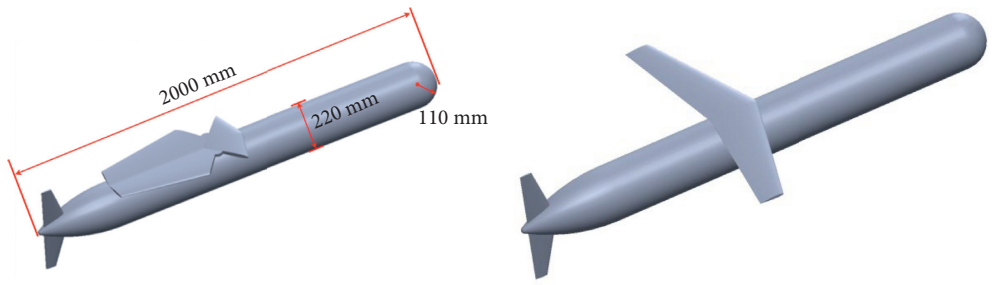

Figure 1: Schematic of the air-launched underwater glider. (a) Wing folded. (b) Wing unfolded.

the load it bears becomes smaller. Then, the wing spreads out, as shown in Figure 1(b). The length of the glider is 2000 mm, the diameter is 220 mm, and the mass is 70.69 kg. The head of the glider is a hemisphere with the radius of 110 mm. When the wing is folded, the gravity centre is on the central axis of the main body, 952 mm away from the head. And in the present study, the glider is regarded as a rigid body.

2.3. Reference Frames. In this study, the inertial frame $O-\mathrm{XYZ}$, the body frame $O_0-X_0Y_0Z_0$, and the velocity frame $V-V_1V_2V_3$ are adopted to describe the motion of the glider and are shown in Figure 2.

The inertial frame $O-\mathrm{XYZ}$ is fixed in the inertial space and an appropriate location on the water surface is selected for the origin O. The $O-X$ axis is horizontal and points to the motion direction of the glider, and the $O-Z$ axis is perpendicular to the water surface and points upwards. The origin of body frame $O_0-X_0Y_0Z_0$ is fixed at the gravity center of the glider, and the O_0-X_0 axis coincides with the longitudinal axis of the glider. The origin of velocity frame $V-V_1V_2V_3$ is also fixed at the gravity centre of the glider, and the $V-V_1$ axis coincides with the velocity vector of the glider. The angle between the $V-V_1$ axis and water surface is defined as the water entry angle θ. And the angle between O_0-X_0 axis and $V-V_1$ axis is defined as the attack angle α, which is positive when the angle $X_0O_0V_1$ is clockwise.

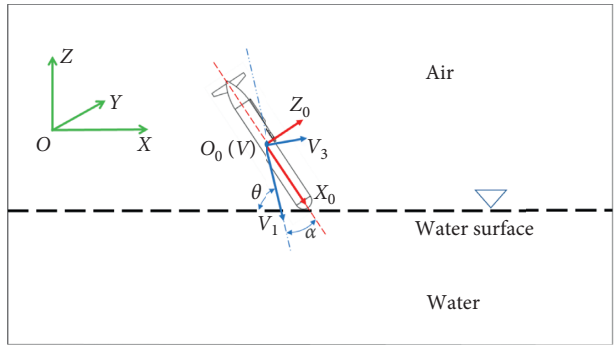

Figure 2: Reference frames.

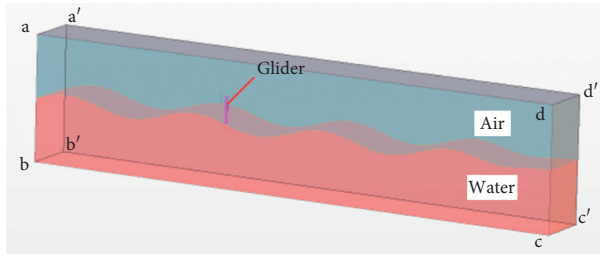

Figure 3: Computational domain.

2.4. Computational Domain. As shown in Figure 3, only half of the domain is meshed as the body is axisymmetric. In the present study, the first order Stokes wave model is used. And the wave length and wave height are set as $\lambda = 10\mathrm{m}$ and $H = 1\mathrm{m}$, respectively.

The surface abb′a′ is set to velocity inlet and 1.5λ away from the glider. The surface cdd′c′ is set to pressure out and 2.5λ away from the glider. A damping zone is set at the pressure outlet boundary to eliminate reflections from boundary. And the damping length is set to 10 m, which is equal to the wave length. The top, bottom, and side boundaries are assigned velocity inlet condition. The water depth is set to 4.5 m, and the height of the air domain is also set to 4.5 m. The SST (Menter) $k-\omega$ turbulence model is selected to simulate the surrounding flow with a grid point for the first cell at $y^+ < 1$. The nondimensional wall distance y^+ is then given by

$$y^+ = \frac{y\rho u_*}{\mu}, \tag{5}$$

where y is the height of the wall adjacent cell centroid from the wall, u_* is the friction velocity, and μ is the dynamic viscosity.

In this study, the hexahedral mesh generated by the cutting mesh generator is used. To clearly simulate the variable process of water entry, fine mesh is assigned to the air-water interface and the region where the glider may pass. Figure 4 shows the partial mesh on the symmetry surface abcd.

3. Discussion on the Numerical Model

3.1. Numerical Method Validation. In this study, the example of the constant-velocity water entry of a sphere is used to verify the numerical method. And the accuracy of the

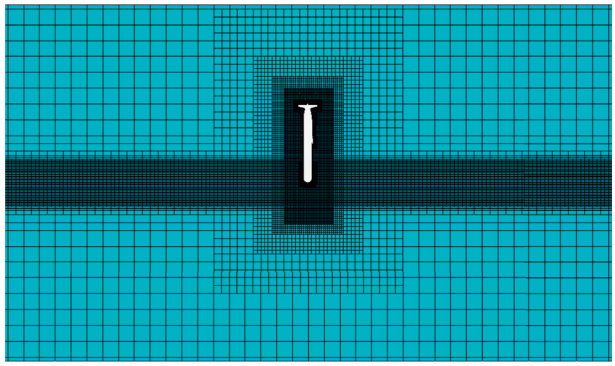

Figure 4: Partial mesh on the symmetry surface.

CFD results was validated by the comparison of nondimensional impact force with the published experimental and numerical results. The nondimensional impact force Cs is defined as

$$\mathbf{Cs} = \frac{2\mathbf{F}}{\rho\pi R^2 \mathbf{V}^2}, \tag{6}$$

where **F** is the total impact force of the sphere, R is the radius of the sphere, And **V** is the water entry velocity of the sphere.

The nondimensional penetration depth of the water entry of the sphere is defined as

$$D^* = \frac{D}{R}, \tag{7}$$

where D is the instantaneous penetration of the sphere.

In this section, the density of water is set to 1000 kg/m^3. The radius of the sphere is set to 110 mm, which is the same size as the glider head. And the water entry velocity is set to 10 m/s.

As shown in Figure 5, the comparison indicates that the vertical impact force obtained from the present model are in good agreement with the experimental data of Nisewanger [22] and Baldwin and Steves [23] and the numerical result by Xiao and Zhang [24]. Finally, the numerical model in this study is proved to be capable of simulating impact force acting on the structure during water entry.

3.2. Convergence Study. The setting of the mesh density and time step will directly affect the accuracy of the numerical results. A case of vertical water entry at the wave peak is used to verify the rationality of the mesh density and time step, as shown in Figure 6. And the impact velocity is set to 10 m/s.

Figure 7 shows the vertical impact force in the direction of $O-Z$ axis with three different mesh densities (coarse: 6.67×10^6; medium: 8.78×10^6; fine: 1.08×10^7). And the time step is set to 1×10^{-5} s for different mesh densities. The vertical impact force with different mesh densities show high consistency. And the mesh configuration with medium density is adopted to predict the impact force during water entry of the glider under wave condition. Then, three time steps are discussed in the time-step

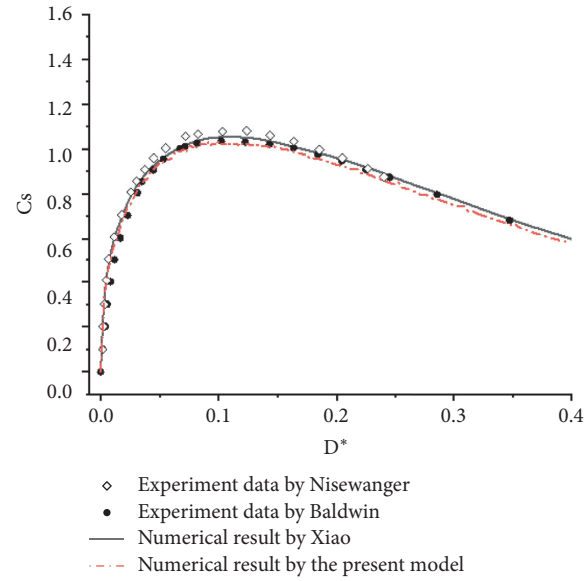

Figure 5: The comparison of nondimensional impact force.

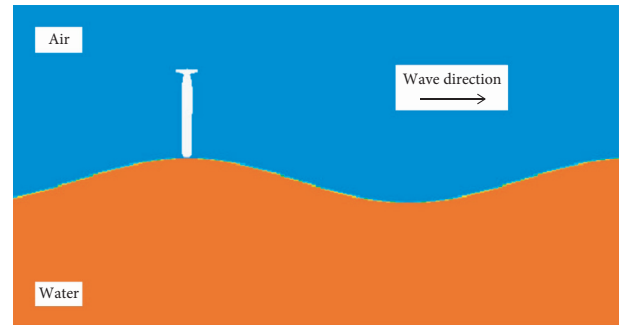

Figure 6: Schematic of convergence study case.

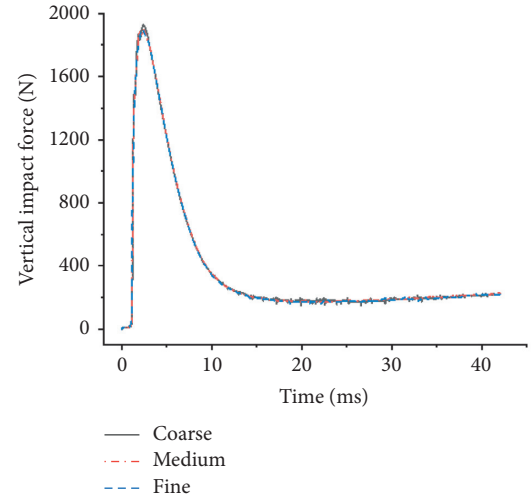

Figure 7: The vertical impact force with different mesh densities.

convergence study. As shown in Figure 8, the results of different time steps are in good convergence. Finally, the time step is set to 1×10^{-5} s in the study of water entry impact force.

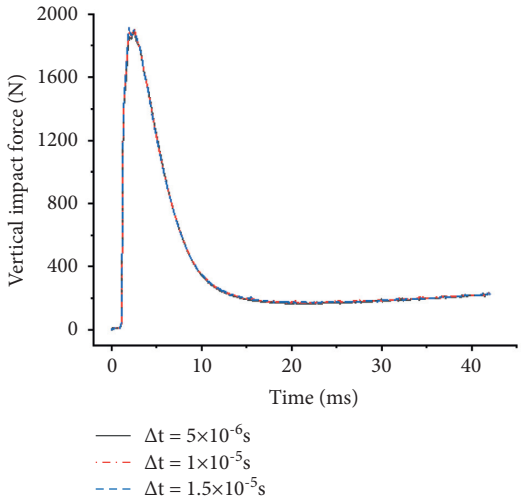

Figure 8: The vertical impact force with different time steps.

4. Results and Discussion

4.1. Influence of Water Entry Point on Impact Force. In this section, four typical water entry points are used to study the influence of water entry point on the impact force, which are the wave peak, the wave trough, and the cross points with the still water level. As shown in Figure 9, the cases that glider vertical water entry at different selected points are marked are Case 1, Case 2, Case 3, and Case 4, respectively.

The impact velocity is set as 10 m/s, and the water entry angle is set as 90 deg. The results of impact forces are shown in Figure 10. The vertical impact forces in the direction of $O-Z$ axis of the glider in Case 1 and Case 3 are almost equal. However, the horizontal forces in the direction of $O-X$ axis of the glider in Case 1 and Case 3 increase gradually in the opposite direction. This is related to the movement of water quality points. According to the first-order Stokes wave model, the horizontal velocity V_x and the vertical velocity V_z of the water quality points is defined as

$$V_x = a\omega\cos(\mathbf{K}\cdot x - \omega t)e^{Kz},$$
$$V_z = a\omega\sin(\mathbf{K}\cdot x - \omega t)e^{Kz}, \quad (8)$$

where a is the wave amplitude, ω is the wave frequency, $\mathbf{K}$ is the wave vector, K is the magnitude of the wave vector, and z is the vertical distance from the mean water level.

The wave surface has different inclination angles in different positions. Therefore, the glider entering the water vertically is subjected to horizontal impact force due to the inclination of the wave surface. At the wave peak and wave trough, the wave surface is horizontal. So, there is no horizontal impact force in the initial of water entry. With the increase of penetration depth, the movement of water quality point makes the glider in Case 1 and Case 3 subject to the opposite force.

In Case 2, the water quality point at the water entry point has the maximum positive vertical velocity. This maximizes the relative impact velocity of the glider. So, the glider in Case 2 has the maximal peak value of vertical impact force. Similarly, due to the minimum relative impact velocity, the glider in Case 4 has the minimal peak value of vertical impact force. In the present wave station and impact velocity, the peak value of the vertical impact force in Case 2 is almost twice the peak value in Case 4. In Case 2 and Case 4, the horizontal impact force is caused by the wave slope. Theoretically, the horizontal impact force of the glider in Case 2 and Case 4 should be symmetrical. However, in the present study, the water entry point is not strictly at the cross point. The water entry point in Case 2 is closer to the cross point, so the peak impact force is greater.

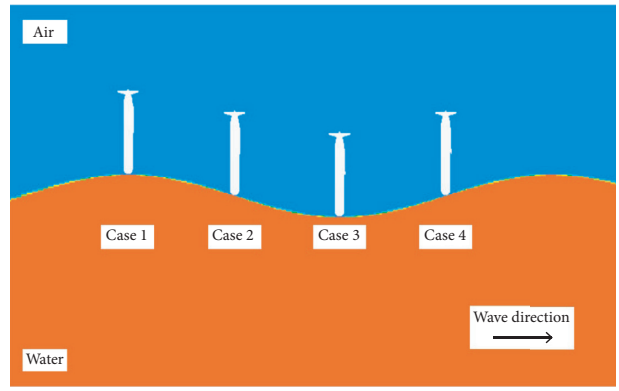

Figure 9: Schematic of vertical water entry at different points.

4.2. Influence of Water Entry Angle on Impact Force. In this section, five water entry angles are used to study the influence of water entry angles on the impact force, which are 80 deg, 90 deg, 100 deg, 110 deg, and 120 deg. According to the results of Section 4.1, the peak values of vertical and horizontal impact force of the glider in Case 2 are both largest. So, the same water entry point as Case 2 is selected. And the water entry velocity is also set to 10 m/s. The results of impact forces are shown in Figure 11. With the increase of water entry angle, the peak value of horizontal impact force increases gradually. This may be because the relative impact velocity in the horizontal direction increases with the increase of water entry angle. With the increase of water entry angle, the peak value of vertical impact force first increases and then decreases. This may be related to the inclination of the wave surface at the water entry point. On the one hand, with the increase of water entry angle, the water entry angle relative to the wave surface at the water entry point is also increasing. This increases the water entry impact force of the glider, and the vertical component of the impact force is also increasing. On the other hand, with the increase of water entry angle, the vertical component of velocity decreases and the vertical component of impact force also decreases. When the water entry angle is less than 100deg, the influence of relative water entry angle is greater, so the peak value of vertical impact force increases. When the water entry angle is 100deg to 110deg, the effects of the opposite effects are basically the same, so the peak value of vertical impact force is basically the same. With the further increase of water entry angle, the influence of vertical component of velocity is greater, so the peak value of vertical impact force decreases. In addition, both the peak values of vertical and horizontal

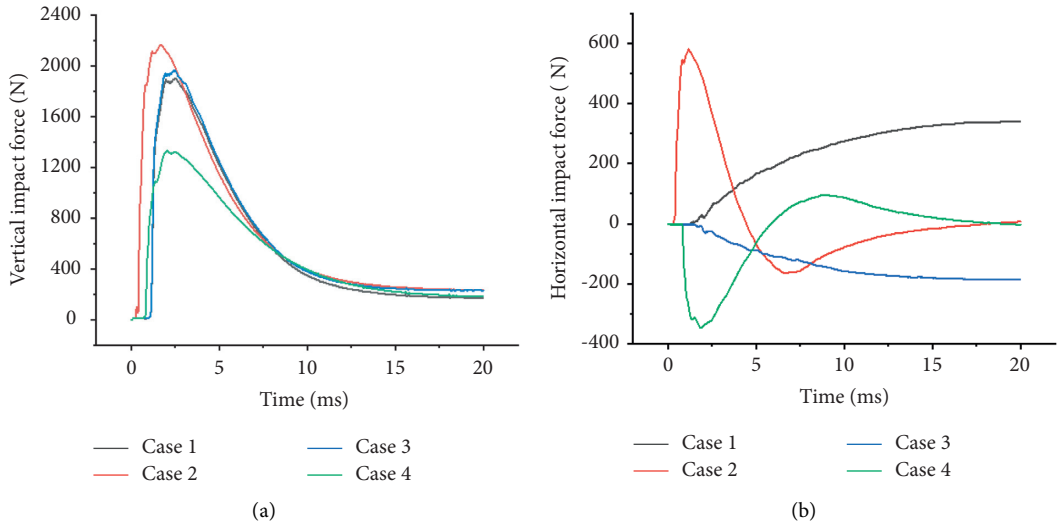

Figure 10: The impact forces with different water entry point. (a) Vertical impact forces. (b) Horizontal impact forces.

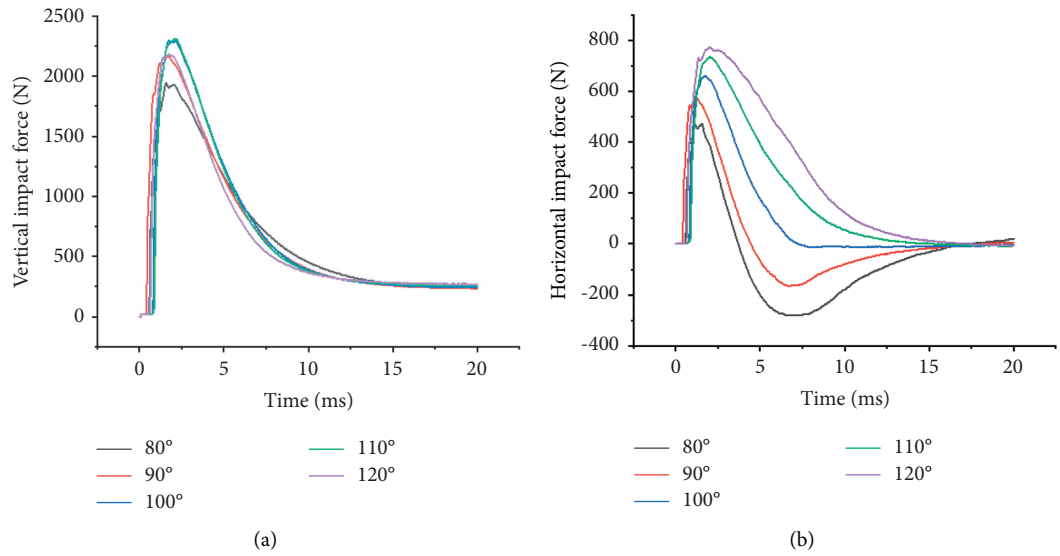

Figure 11: The impact forces with different water entry angles. (a) Vertical impact forces. (b) Horizontal impact forces.

impact force are bigger when the water entry angle is greater than 90 deg. Therefore, a water entry angle less than 90deg is a better choice.

4.3. Influence of the Attack Angle on Impact Force. In this section, five water entry attack angles are used to study the influence of attack angle on the impact force, which are −10 deg, −5 deg, 0 deg, 5 deg, and 10 deg. According to the results of Section 4.2, the peak values of vertical and horizontal impact force of the glider when the water entry angle is 110 deg are both largest. So, the same water entry point as Case 2 is selected, the water entry angle is set to 110 deg, and the water entry velocity is also set to 10 m/s. The results of impact forces are shown in Figure 12. The attack angle has little effect on the peak impact force. This may be because the glider's head is hemispherical. Then, the horizontal and vertical forces on the glider tend to be stable under different attack angles. In general, the attack angle has little effect on the peak impact force of the glider at the set entry attitude.

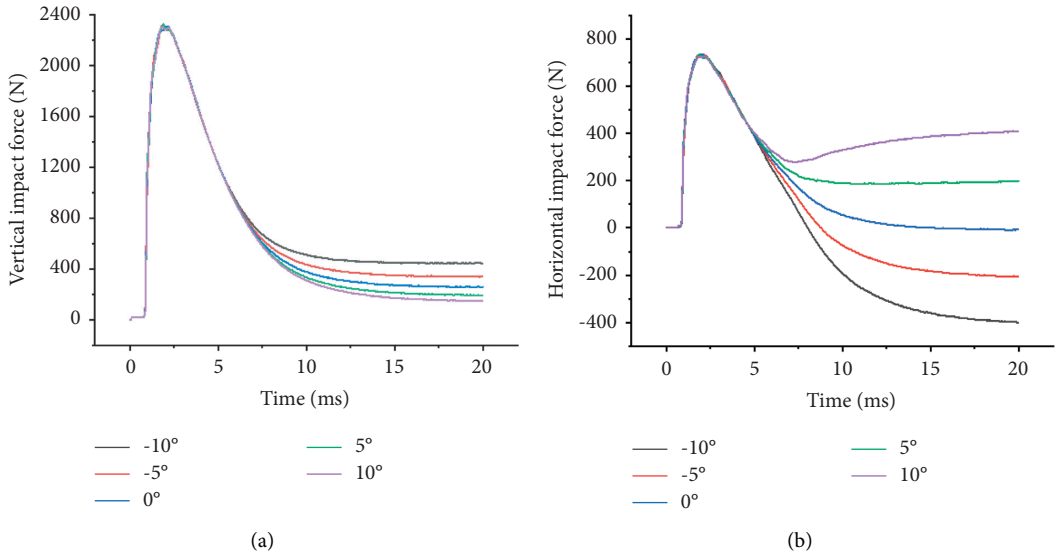

Figure 12: The impact forces with different attack angle. (a) Vertical impact forces. (b) Horizontal impact forces.

5. Conclusions

In this study, the water entry impact forces of an air-launched underwater glider under wave conditions are analyzed by numerical simulation. These results could be helpful to the design of air-launched underwater gliders. By studying the influence of water entry points, water entry angles, and attack angles on the impact force, we arrive at the following conclusions:

(1) The water entry points have a great influence on the peak value of vertical impact force. When the impact velocity is 10 m/s, the peak value of vertical impact force when water entry point is on the right side of wave peak and intersects with the still water level is almost twice the peak value when water entry at the intersection point on the left side of wave peak.

(2) The water entry angle has a great influence on the peak value of horizontal impact force when the water entry point intersects with the still water level. This is mainly related to the horizontal component of impact velocity. The greater the horizontal component of impact velocity, the greater the peak value of impact force.

(3) It should be avoided that the water entry direction is opposite to the wave direction, which makes the glider suffer greater impact force than along the wave direction.

(4) For the air-launched underwater glider with hemispherical head, the attack angle has little effect on the peak impact force.

Data Availability

The data used to support the findings of this study are included within the article.

Conflicts of Interest

The authors declare that they have no conflicts of interest.

Acknowledgments

This work was supported by the National Science Foundation of China (Grant no. 51709030); the State Key Laboratory of Ocean Engineering, Shanghai Jiao Tong University (Grant no. 1904), Natural Science Foundation of Liaoning Province in 2020 (Grant no. 2020-MS-125), the Fundamental Research Funds for the Central Universities (Grant nos. 3132021120 and 3132022123), and the Dalian High Level Talents Innovation Support Plan (2019RQ068).

References

[1] J-C Yu, A-Q Zhang, W-m Jin, Q. Chen, Y. Tian, and C-j Liu, "Development and experiments of the Sea-Wing underwater glider," *China Ocean Engineering*, vol. 25, no. 4, pp. 721–736, 2011.

[2] G. X. Yan, G. Pan, Y. Shi, L-M Chao, and D. Zhang, "Experimental and numerical investigation of water impact on air-launched AUVs," *Ocean Engineering*, vol. 167, pp. 156–168, 2018.

[3] A. Z. Chaudhry, Y. Shi, and G. Pan, "Study on the oblique water entry impact performance of AUV under different launch conditions based on coupled FEM-ALE method," *AIP Advances*, vol. 10, no. 11, Article ID 115020, 2020.

[4] T. V. Karman, *The Impact of Seaplane Floats during landing*, Technical Report Archive & Image Library, 1929.

[5] H. Wagner, "Phenomena associated with impacts and sliding on liquid surfaces," *Journal of Applied Mathematics and Mechanics*, vol. 12, no. 4, 1932.

[6] T. Miloh, "On the initial-stage slamming of a rigid sphere in a vertical water entry," *Applied Ocean Research*, vol. 13, no. 1, 1991.

[7] A. A. Korobkin, "The entry of an elliptical paraboloid into a liquid at variable velocity," *Pmm Journal of Applied Mathematics and Mechanics*, vol. 66, no. 1, 2002.
[8] A. Tassin, N. Jacques, A. E. M. Alaoui, A. Nême, and B. Leblé, "Assessment and comparison of several analytical models of water impact," *The International Journal of Multiphysics*, vol. 4, no. 2, pp. 125–140, 2010.
[9] N. Aquelet, M. Souli, and L. Olovsson, "Euler-Lagrange coupling with damping effects: application to slamming problems," *Computer Methods in Applied Mechanics and Engineering*, vol. 195, pp. 1–3, 2006.
[10] R. Panciroli, S. Abrate, G. Minak, and A. Zucchelli, "Hydroelasticity in water-entry problems: comparison between experimental and SPH results," *Composite Structures*, vol. 94, no. 2, pp. 532–539, 2012.
[11] A. L. Facci, M. Porfiri, and S. Ubertini, "Three-dimensional water entry of a solid body: a computational study," *Journal of Fluids and Structures*, vol. 66, 2016.
[12] M. Liu, L. Tan, and S. Cao, "Cavitation-Vortex-turbulence interaction and one-dimensional model prediction of pressure for hydrofoil ALE15 by large eddy simulation," *Journal of Fluids Engineering-Transactions of the Asme*, vol. 141, no. 2, 2019.
[13] M. Liu, L. Tan, Y. Liu, Y. Xu, and S. Cao, "Large eddy simulation of cavitation vortex interaction and pressure fluctuation around hydrofoil ALE 15," *Ocean Engineering*, vol. 163, pp. 264–274, 2018.
[14] M. Liu, L. Tan, and S. Cao, "Dynamic mode decomposition of cavitating flow around ALE 15 hydrofoil," *Renewable Energy*, vol. 139, 2019.
[15] C. Li, C. Wang, Y. Wei, and W. Xia, "Three-dimensional numerical simulation of cavity dynamics of a stone with different spinning velocities," *International Journal of Multiphase Flow*, vol. 129, Article ID 103339, 2020.
[16] Y. Shi, G. Pan, G. X. Yan, S. C. Yim, and J. Jiang, "Numerical study on the cavity characteristics and impact loads of AUV water entry," *Applied Ocean Research*, vol. 89, pp. 44–58, 2019.
[17] A. Z. Chaudhry, G. Pan, and Y. Shi, "Numerical evaluation of the hydrodynamic impact characteristics of the air launched AUV upon water entry," *Modern Physics Letters B*, vol. 34, no. 14, 2020.
[18] G. X. Yan, G. Pan, and Y. Shi, "Ricochet characteristics of AUVs during small-angle water entry process," *Mathematical Problems in Engineering*, vol. 2019, Article ID 9518437, 12 pages, 2019.
[19] D. Qi, J. Feng, B. Xu, J. Zhang, and Y. Li, "Investigation of water entry impact forces on airborne-launched AUVs," *Engineering Applications of Computational Fluid Mechanics*, vol. 10, no. 1, pp. 473–484, 2016.
[20] X. H. Wang, Y. Shi, G. Pan, X. Chen, and H. Zhao, "Numerical research on the high-speed water entry trajectories of AUVs with asymmetric nose shapes," *Ocean Engineering*, vol. 234, Article ID 109274, 2021.
[21] P. Yu, C. Shen, C. Zhen, H. Tang, and T. Wang, "Parametric study on the free-fall water entry of a sphere by using the RANS method," *Journal of Marine Science and Engineering*, vol. 7, no. 5, p. 122, 2019.
[22] C. Nisewanger, *Experimental Determination of Pressure Distribution on a Sphere during Water Entry*, Naval Ordnance Test Station China Lake CA, Ridgecrest, CA, USA, 1961.
[23] J. L. Baldwin and H. K. Steves, "Vertical water entry of spheres," *NASA STI/Recon Technical Report N*, vol. 76, 1975.
[24] H. Xiao and X. Zhang, "Numerical investigation of the fall rate of a sea-monitoring probe," *Ocean Engineering*, vol. 56, 2012.